Fracture alteration by precipitation resulting from thermal gradients: Upscaled mean aperture-effective transmissivity relationship

A. Chaudhuri,[1] H. Rajaram,[2] and H. Viswanathan[3]

Received 2 June 2011; revised 6 October 2011; accepted 29 November 2011; published 18 January 2012.

[1] Precipitation and dissolution reactions in fractures alter apertures, which in turn affects their flow and transport properties. We consider aperture alteration by precipitation in a "gradient-reaction" regime where fluids are close to chemical equilibrium with a mineral everywhere, but precipitation is driven by solubility gradients. Monte Carlo simulations on computer-generated aperture fields suggest that the most important feature of fracture alteration by precipitation is the formation of elongated precipitate bodies perpendicular to the mean flow direction. The simulation results provide a basis for a proposed upscaling relationship between mean aperture and the effective transmissivity tensor, incorporating a critical aperture at which the transmissivity decreases steeply.

Citation: Chaudhuri, A., H. Rajaram, and H. Viswanathan (2012), Fracture alteration by precipitation resulting from thermal gradients: Upscaled mean aperture-effective transmissivity relationship, *Water Resour. Res.*, *48*, W01601, doi:10.1029/2011WR010983.

1. Introduction

[2] The transmissivity of fractured rock masses is often dominated by fractures. Alteration of fracture aperture and transmissivity by dissolution and precipitation reactions is relevant in the context of several geological processes and the long-term behavior of geothermal energy [*Jing et al.*, 2002], nuclear waste storage [*Dobson et al.*, 2003], and subsurface carbon sequestration systems [*Shao et al.*, 2010]. One important regime of reactive fracture alteration is the "gradient reaction" regime [*Phillips*, 1991], wherein dissolution and precipitation occur due to flow across solubility gradients, often induced by temperature gradients. In this technical note we consider the relationship between mean aperture and effective transmissivity of rough-walled (variable-aperture) fractures during precipitation in gradient reaction regimes. For silica and quartz, whose solubility increases with temperature (below 340°C), precipitation will occur if the temperature decreases along a flow path, (e.g., in the far field region of a heat generating nuclear waste repository [*Langmuir*, 1987]). For minerals whose solubility decreases with temperature, such as calcite, precipitation will occur if the temperature increases along a flow path [e.g., *Bächler and Kohl*, 2005].

[3] The simple parallel-plate model leads to cubic dependence between aperture and transmissivity, and has been used to represent the influence of dissolution/precipitation in gradient reaction regimes [*Nimblett and Ruppel*, 2003]. However, experimental studies of precipitation under gradient-reaction conditions have shown that permeability decreases substantially even for small amounts of precipitation [e.g., *Vaughan*, 1985]. *Verma and Pruess* [1988] explained this behavior based on a model of fractures in series, invoking the clogging of narrow fracture apertures. They showed that clogging of narrow fracture apertures produces a steeper reduction in transmissivity than predicted by the parallel-plate model. In experiments involving kinetic precipitation in fractures, *Singurindy and Berkowitz* [2005] observed that transmissivity decreased at a faster rate in rough-walled fractures than in smooth-walled fractures. The numerical simulations of *Chaudhuri et al.* [2008] demonstrated that in variable-aperture fractures, precipitation in gradient reaction regimes leads to the formation of elongate precipitate bands perpendicular to the flow direction, resulting in a steep reduction of transmissivity with mean fracture aperture. In this technical note we show that the formation of elongation precipitation bands is an inherent feature of the behavior in variable aperture fractures across a broad range of initial fracture geometries. We also propose a simple form for the upscaled relationship between mean fracture aperture and effective transmissivity that produces the steep reduction in effective transmissivity observed in numerical simulations.

2. Computational Approach

[4] Aperture alteration can be described using quasi-steady-state flow and transport equations due to the large ratio between the mineral mass density and aqueous solubility [*Ortoleva et al.*, 1987; *Chaudhuri et al.*, 2008]. In gradient reaction regimes, the kinetics of precipitation reactions are relatively fast; thus fluid concentrations are assumed to be at the solubility limit (C_s) and precipitation is driven by reduction in solubility along a flow path. Under

[1]Department of Applied Mechanics, Indian Institute of Technology Madras, Chennai 36 Tamil Nadu, India.
[2]Department of Civil, Environmental and Architectural Engineering, University of Colorado, Boulder, Colorado, USA.
[3]Earth and Environmental Sciences Division, Los Alamos National Laboratory, Los Alamos, New Mexico, USA.

0043-1397/12/2011WR010983

these conditions, aperture alteration can be described by the following equations [*Chaudhuri et al.* 2008]:

$$\omega\rho_r \frac{\partial b}{\partial t} = \mathbf{q} \cdot \nabla C_s, \tag{1a}$$

where

$$\mathbf{q} = -\frac{b^3 g}{12\nu}\nabla h. \tag{1b}$$

[5] In (1a), $b(x,z)$ is the aperture, with x and z denoting coordinates in the fracture plane; $\mathbf{q}(x,z)$ is the fluid flux, given by the local cubic law in (1b), where g is the gravitational constant, ν is the kinematic viscosity of water and $h(x,z)$ denotes the head field; $\omega\rho_r$ denotes the number of moles of the precipitating mineral per unit volume of rock. In (1a) the dissolved mineral mass flux is assumed to be advection dominated (see *Chaudhuri et al.* [2008] for a justification). The fluid mass balance equation is given by

$$\nabla \cdot \mathbf{q} = \nabla \cdot \left(-\frac{b^3 g}{12\nu}\nabla h\right) = 0. \tag{2}$$

In a variable-aperture fracture there are spatial variations in b and hence in q as a result of which there are spatial variations in the aperture alteration rate ($\partial b/\partial t$). As the aperture field evolves due to precipitation, the fluid flux field is further altered. Elongated precipitation bands perpendicular to mean flow result from this feedback. We consider fractures subject to a constant mean hydraulic gradient along any direction (z, not to be confused with vertical) with periodic boundary conditions on the lateral edges parallel to the mean hydraulic gradient. The solubility gradient is oriented along the flow direction and assumed to be constant in space and time, corresponding to a conductive heat transfer regime. Evolution of fracture aperture by precipitation was simulated in a square domain of size ($L \times L$) discretized with 1024×1024 grid points, and involves recalculation of the head and flux fields from (2) with (1b), explicitly coupled to aperture alteration (1a).

3. Results and Discussion

[6] The formation of elongated precipitate bodies is explained by the dependence of the precipitation rate on the magnitude and direction of the flux in a gradient reaction system. As the flow gets diverted around a low-transmissivity obstacle, the flow rate is high in the streamline that is just outside the obstacle. However, in the portion of the streamline where the flux vector is perpendicular to the temperature/solubility gradient, little precipitation occurs. As the streamline straightens out at the lateral edges of the obstacle, the flux becomes aligned with the solubility gradient and results in large precipitation rates. The precipitation rate in this streamline is higher than in adjacent streamlines that are flowing through higher-transmissible regions, because it carries a larger flux. Thus, there is more precipitation at the lateral edges of a low-transmissivity obstacle and it grows preferentially in a direction perpendicular to the mean flux.

[7] We illustrate this mechanism in an idealized variable-aperture fracture, with a regular array of low aperture lenses oriented perpendicular to mean flow (and solubility gradient). These lenses appear as dark patches in Figure 1a. The streamlines in the figure illustrate the flux variations resulting from the low-transmissivity lenses. In rows containing lenses there is a higher flux in the space between low-aperture lenses due to flow diversion. As a result, the highest precipitation rates occur in these spaces between low-aperture lenses. Thus each row of low-aperture lenses becomes an elongated low-aperture band which can be identified as a dark patch in Figure 1b. Due to formation of these elongated bands the overall transmissivity of the fracture approaches zero, reducing the flux transmitted by the fracture. Thus the aperture reduction rate also reduces and approaches zero. However, the aperture reduction rate between rows of initial low transmissivity lenses is always lower because the flux is smaller, and apertures remain larger in these regions. As the effective transmissivity approaches zero, the flux to these regions is also reduced and at some stage the aperture in these regions does not decrease further. Thus, the mean aperture approaches a constant nonzero value, while the effective transmissivity approaches zero. This is an important feature of the mean aperture versus effective transmissivity relationship that is not captured by the cubic dependence implicit in parallel-plate fracture models. We show below that similar behavior arises in random aperture fields.

[8] The effective transmissivity of variable-aperture fractures depends on the degree of aperture variability (quantified by the coefficient of variation $\sigma_0^2/\overline{b}_0^2$ of the initial aperture field, where $\overline{b}_0$ and σ_0^2 represent the initial mean and variance of the aperture field) and correlation

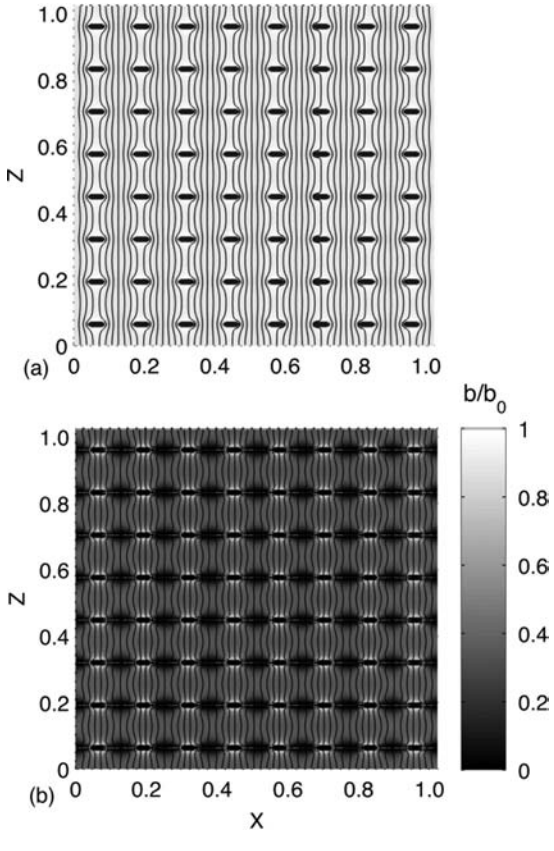

Figure 1. Aperture alteration and barrier formation in an initial aperture field with a regular array of low-aperture patches. (a) Initial and (b) late-time aperture fields with streamlines.

structure (quantified by the correlation functions and correlation lengths λ_x and λ_z in the x and z directions) [*Gelhar*, 1993; *Zimmerman and Bodvarsson*, 1996]. Our numerical simulations demonstrate the influence of the above measures of aperture variability on the pattern formation due to precipitation. Although fractal/power law spectral density functions have been proposed for fracture surfaces, observations suggest a low-wave number cutoff, below which power law behavior is not observed for aperture spectra [e.g., *Brown*, 1995]. A review paper by *Molz et al.* [2005] also notes that power law behavior is seldom observed over a range greater than about two decades in wave number space. Power law spectra with low wave number cutoffs are essentially stationary random fields. *Lanaro* [2005] also demonstrated that the standard deviation of measured fracture aperture fields becomes constant above a threshold length scale. We thus used a stationary random field model for the fracture aperture field. Specifically, the following 2-D Gaussian hole type spectral density function was used for the initial aperture field:

$$S_{bb}(\mathbf{k},0) = \frac{\sigma_0^2 \lambda_x \lambda_z}{4\pi}\,(k_x^2\lambda_x^2 + k_z^2\lambda_z^2)\exp\left(-\frac{k_x^2\lambda_x^2 + k_z^2\lambda_z^2}{2}\right), \quad (3)$$

Three different spatial correlation structures of the initial aperture field (as shown in Figure 2) were considered (L is the domain size): (a) isotropic $\lambda_x = 0.01L$ and $\lambda_z = 0.01L$, (b) longitudinal anisotropic $\lambda_x = 0.01L$ and $\lambda_z = 0.05L$, and (c) transverse anisotropic $\lambda_x = 0.05L$ and $\lambda_z = 0.01L$. We performed simulations of 100 realizations for each case with different $\sigma_0^2/\overline{b}_0^2$ for the three different initial correlation structures. Random field realizations were generated using a Fast Fourier Transform (FFT) spectral method. Results are presented in dimensionless form below. With the initial aperture-integrated mean flux denoted as q_0, a dimensionless time can be defined as $tq_0/\,(L\overline{b}_0)$. Figures 2a2–2c2 show the dimensionless aperture field $b/\overline{b}_0$ (from a single realization) at a large dimensionless time $tq_0/(L\overline{b}_0) \approx 10^5$ for the three different cases. In all cases, elongated bands of low aperture form perpendicular to the flow. It is noteworthy that the elongate barriers perpendicular to flow form even when the aperture field has a longer correlation length in the direction of mean flow and solubility gradient. Eventually a few isolated dominant barriers form in all cases, similar to the behavior noted by *Chaudhuri et al.* [2008]. Due to the formation of elongated barriers, the effective transmissivity approaches zero in all cases, even though the mean aperture approaches a constant nonzero value. As noted above, the mean aperture approaches a constant value because flow is diverted around some large-aperture regions, and these regions thus remain unaltered (compare upper and lower figures in Figure 2, e.g., b1 and b2).

[9] The time-evolving ensemble-averaged effective transmissivity is plotted against the time-evolving mean aperture during fracture alteration in Figures 3a–3c in terms of $\log(T_{\text{eff}}/T_{\text{eff}}(t=0))$ versus $\log(\overline{b}/\overline{b}_0)$. The behavior in

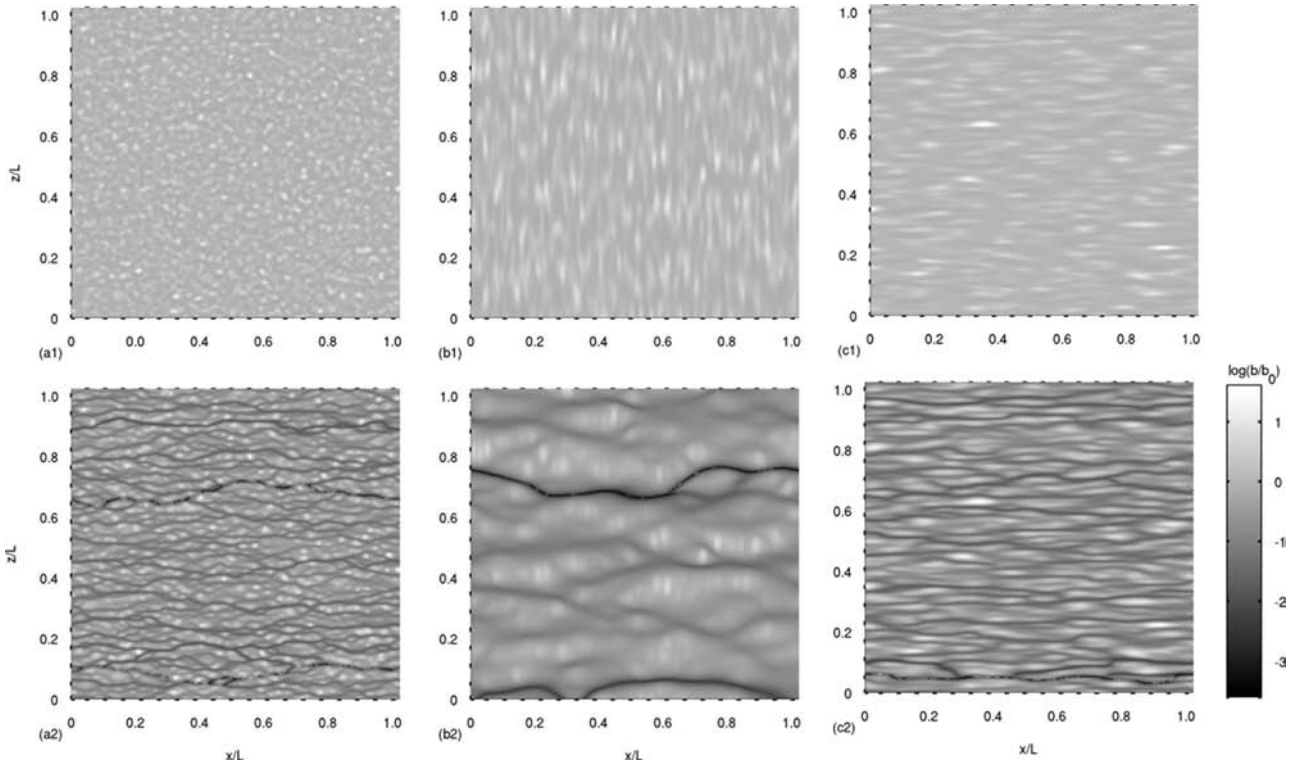

Figure 2. Initial (top) and late-time (bottom) aperture fields for different initial aperture correlation structures. (a1, a2) Isotropic with $(\lambda_x/L = \lambda_z/L = 0.01)$; (b1, b2) longitudinally anisotropic with $\lambda_x/L = 0.01, \lambda_z/L = 0.05$; and (c1, c2) transversely anisotropic with $\lambda_x/L = 0.05, \lambda_z/L = 0.01$. The mean flow is along the z direction. All cases show the formation of barriers perpendicular to mean flow.

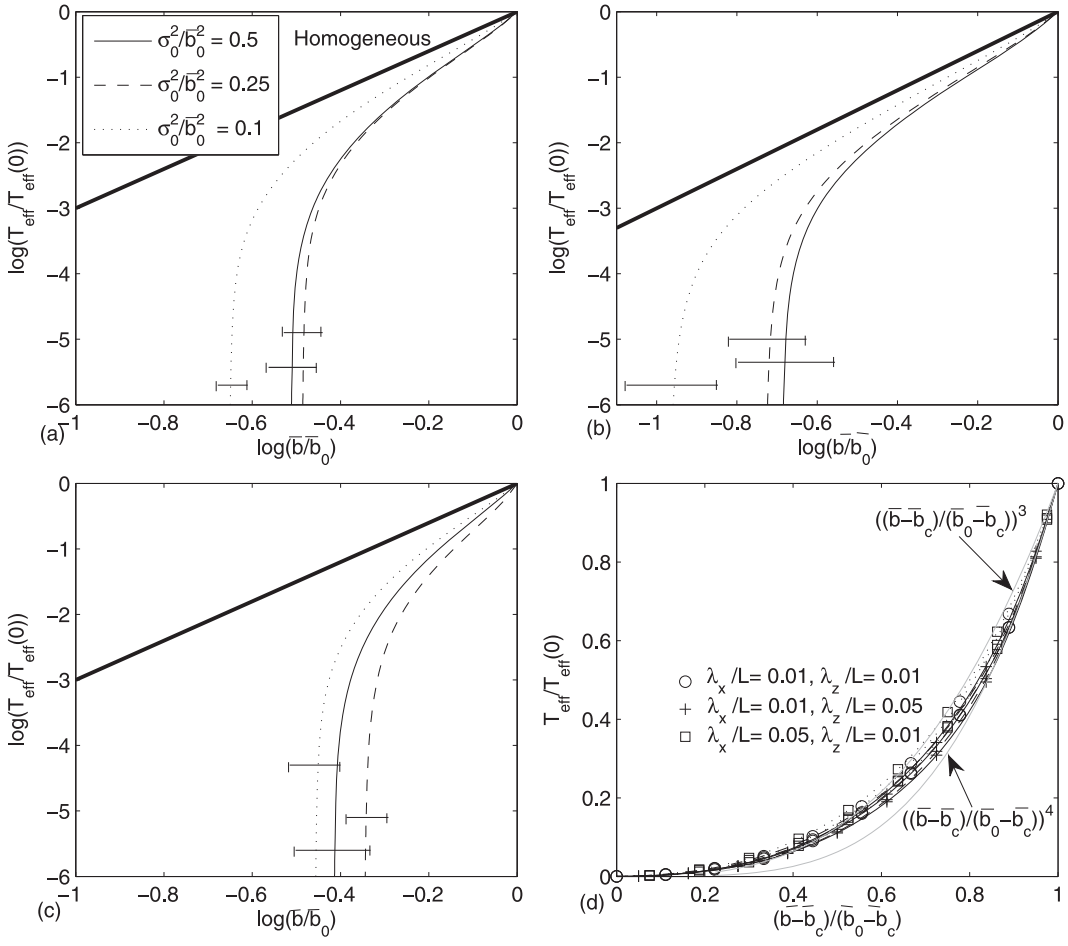

Figure 3. Time evolution of effective transmissivity and mean aperture during precipitation for (a) isotropic, (b) longitudinally anisotropic, and (c) transversely anisotropic initial aperture fields with different $\sigma_b/\overline{b}_0$. The effective transmissivity-mean aperture relationship is plotted as a function of $(\overline{b}-\overline{b}_c)/(\overline{b}_0-\overline{b}_c)$ in (d). The dark line in (a), (b), and (c) shows the cubic relationship in a parallel-plate fracture.

parallel-plate fractures is also shown for reference. For all three cases we observe a steep decline in effective transmissivity at a critical value of $\overline{b}_c/\overline{b}_0$ (mean values of $\overline{b}_c/\overline{b}_0$ are reported in Table 1). The critical value of $\overline{b}_c/\overline{b}_0$ varies with $\sigma_0^2/\overline{b}_0^2$ and the initial correlation structure (i.e., λ_x/λ_z). For $\sigma_0^2/\overline{b}_0^2 = 0.1$, $\overline{b}_c/\overline{b}_0$ is smaller than for $\sigma_0^2/\overline{b}_0^2 = 0.25$ and 0.5 (which are not very different). The decrease in the $\overline{b}_c/\overline{b}_0$ with $\sigma_0^2/\overline{b}_0^2$ makes sense, as $\overline{b}_c/\overline{b}_0$ is zero for the parallel-plate case. For a fixed $\sigma_0^2/\overline{b}_0^2$, $\overline{b}_c/\overline{b}_0$ increases systematically as the anisotropy ratio λ_x/λ_z increases (Figure 3, Table 1). This behavior results because larger regions of the fracture experience low rates of fracture alteration, as the flux deviates away from the direction of the solubility gradient to get around the initially elongated low-transmissivity regions. The spread covered by realizations for each case are shown with an error bar. For very small $\sigma_0^2/\overline{b}_0^2$, the spread is tight so that the mean behavior is distinguishable from other cases. However for moderate to large $\sigma_0^2/\overline{b}_0^2$, the spreads overlap, suggesting that the systematic variation of $\overline{b}_c/\overline{b}_0$ with $\sigma_0^2/\overline{b}_0^2$ may not predict the behavior in individual realizations accurately.

[10] The simulation results suggest that the steep reduction of effective transmissivity at some critical value of $\overline{b}_c/\overline{b}_0$ is a universal and important feature of the behavior during precipitation in variable-aperture fractures, which should be incorporated in upscaled relationships between effective transmissivity and mean aperture in large-scale models. In Figure 3d we plot the time-evolving $T_{\text{eff}}/T_{\text{eff}}(0)$ versus $(\overline{b}-\overline{b}_c)/(\overline{b}_0-\overline{b}_c)$ for all simulated cases. The collapse of the curves for the different cases suggests an effective transmissivity-mean aperture relation of the form

$$\frac{T_{\text{eff}}}{T_{\text{eff}}(t=0)} = \left(\frac{\overline{b}-\overline{b}_c}{\overline{b}_0-\overline{b}_c}\right)^n, \tag{4}$$

where $n \approx 3$. This relationship is also valid for parallel-plate fractures as $\overline{b}_c = 0$ for this case. The variation of

Table 1. Dimensionless Critical Aperture $\overline{b}_c/\overline{b}_0$ for Various Cases

Correlation	$\sigma_0^2/\overline{b}_0^2 = 0.1$	$\sigma_0^2/\overline{b}_0^2 = 0.25$	$\sigma_0^2/\overline{b}_0^2 = 0.5$
$\lambda_x/L = 0.01$, $\lambda_z/L = 0.01$	0.22	0.33	0.31
$\lambda_x/L = 0.01$, $\lambda_z/L = 0.05$	0.11	0.19	0.21
$\lambda_x/L = 0.05$, $\lambda_z/L = 0.01$	0.35	0.45	0.39

$\overline{b}_c/\overline{b}_0$ across the different cases from Table 1 is approximately between 0.1 (low initial aperture variance, longer correlation parallel to mean flow and solubility gradient) and 0.4 (higher initial aperture variance, longer correlation perpendicular to mean flow and solubility gradient). The upscaled relationship (4) is empirically derived from the simulation results. Although effective transmissivity-mean aperture relationships have been derived from stochastic analysis incorporating the influence of aperture variability [*Zimmerman and Bodvarsson*, 1996; *Gelhar*, 1993], these analyses are typically valid for small aperture variance and restricted forms of the aperture probability density function. Reproducing the behavior indicated by (4) using a stochastic perturbation analysis is an interesting and challenging problem for future research, particularly due to unusually skewed late-time aperture pdfs revealed in the numerical simulations (also see Figure 7 in *Chaudhuri et al.* [2008]).

4. Conclusions

[11] For fracture alteration by precipitation in gradient-reaction regimes, a steep reduction in effective transmissivity at a critical value of the mean aperture ($\overline{b}_c/\overline{b}_0$) seems to be the most important and universal feature that should be represented in upscaled effective transmissivity versus mean aperture relationships. A simple relationship of the form (4) appears to satisfactorily represent behavior across a wide range of initial aperture statistics. The parameter ($\overline{b}_c/\overline{b}_0$) in (4) varies systematically between 0.1 and 0.4 depending on the initial correlation anisotropy, which may be approximately related to the stress state during fracturing (e.g., tensile versus shear fractures produce different degrees and types of anisotropy, [*Auradou et al.*, 2005; *Mallikamas and Rajaram*, 2005]). Thus (4) may be used to represent the reduction in fracture transmissivity in models of enhanced geothermal and CO_2 injection systems, with prescribed values of ($\overline{b}_c/\overline{b}_0$) based on estimates of the initial mean aperture, aperture variance, and stress state during fracturing. For fractures with high degree of aperture variability (e.g., $\sigma_0^2/\overline{b}_0^2 > 0.25$), there is considerable variation in ($\overline{b}_c/\overline{b}_0$) between individual realizations, which implies some uncertainty in the assignment of ($\overline{b}_c/\overline{b}_0$) values for applications. Although our analysis pertains to a gradient-reaction regime, experimental studies under more complex chemical conditions with kinetic precipitation [e.g., *Singurindy and Berkowitz*, 2005] also suggest a similar rapid decrease in transmissivity of variable-aperture fractures. Establishment of a theoretical basis for (4), improved understanding of the factors controlling ($\overline{b}_c/\overline{b}_0$), investigation of the behavior in networks with varying orientations, and extensions to more complex systems with kinetic precipitation are important problems for future research.

[12] **Acknowledgments.** We gratefully acknowledge financial support from the Institute for Geophysics and Planetary Physics at Los Alamos National Laboratory (grant number IGPP Geo 1714). We thank the Associate Editor Walter Illman, Jerry Fairley, Daniel Fernandez-Garcia, and an anonymous reviewer for their careful reviews.

References

Auradou, H., G. Drazer, J. P. Hulin, and J. Koplik (2005), Permeability anisotropy induced by the shear displacement of rough fracture walls, *Water Resour. Res.*, *41*, W09423, doi:10.1029/2005WR003938.

Bächler, D., and T. Kohl (2005), Coupled thermal-hydraulic-chemical modeling of enhanced geothermal systems, *Geophys. J. Int.*, *161*(2), 533–548.

Brown, S. R. (1995), Simple mathematical model of a rough fracture, *J. Geophys. Res.*, *100*(B4), 5941–5952.

Chaudhuri, A., H. Rajaram, and H. Viswanathan (2008), Alteration of fractures by precipitation and dissolution in gradient reaction environments: Computational results and stochastic analysis, *Water Resour. Res.*, *44*, W10410, doi:10.1029/2008WR006982.

Dobson, P. F., T. J. Kneafsey, E. L. Sonnenthal, N. Spycher, and J. A. Apps (2003), Experimental and numerical simulation of dissolution and precipitation: Implications for fracture sealing at Yucca Mountain, *Nevada J. Contam. Hydrol.*, *6263*, 459–476.

Gelhar, L. W. (1993), *Stochastic Subsurface Hydrology*, Prentice-Hall, Upper Saddle River, NJ.

Jing, Z., K. Watanabe, J. Willis-Richards, and T. Hashida (2002), A 3-D water/rock chemical interaction model for prediction of HDR/HWR geothermal reservoir performance, *Geothermics*, *31*(1), 1–28.

Lanaro F. (2000), A random field model for surface roughness and aperture of rock fractures, *Int. J. Rock Mech. Min. Sci.*, *37*, 1195–1210.

Langmuir D. (1987), Overview of coupled processes with emphasis in geochemistry, *Coupled Processes Associated With Nuclear Waste Repositories*, edited by C. F. Tsang, pp. 67–101, Academic, New York.

Mallikamas, W., and H. Rajaram (2005), On the anisotropy of the aperture correlation and effective transmissivity in fractures generated by sliding between identical self-affine surfaces, *Geophys. Res. Lett.*, *32*, L11401, doi:10.1029/2005GL022859.

Molz, F. J., M. M. Meerschaert, T. J. Kozubowski, and P. D. Hyden (2005), Do heterogeneous sediment properties and turbulent velocity fluctuations have something in common? Some history and a new stochastic process, in *Dynamics of Fluids and Transport in Fractured Rock, Geophys. Monogr. Ser.*, vol. 162, edited by B. Faybishenko, P. A. Witherspoon, and J. Gale, pp. 13–22 American Geophysical Union, Washington, DC.

Nimblett, J., and C. Ruppel (2003), Permeability evolution during the formation of gas hydrates in marine sediments, *J. Geophys. Res.*, *108*(B9), 2420, doi:10.1029/2001JB001650.

Ortoleva, P., M. Enrique, C. Moore, and J. Chadam (1987), Geochemical self-organization I: Reaction-transport feedbacks and modeling approach, *Am. J. Sci.*, *287*, 979–1007.

Phillips, O. M. (1991), *Flow and Reactions in Permeable Rocks*, Cambridge Univ. Press, Cambridge.

Shao, H., J. R. Ray and Y.-S. Jun (2010), Dissolution and precipitation of clay minerals under geologic CO_2 sequestration conditions: CO_2-brine-phlogopite interactions, *Environ. Sci. Technol. 44*(15), 5999–6005.

Singurindy, O., and B. Berkowitz (2005), The role of fracture on coupled dissolution and precipitation patterns in carbonate rocks, *Adv. Water Resour.*, *28*, 507–521.

Vaughan, P. J. (1985), Analysis of permeability reduction during flow of heated, aqueous fluid through westerly granite, in International Symposium on Coupled Processes Affecting the Performance of a Nuclear Waste Repository, Lawrence Berkeley Laboratory, Sponsored by U.S. DOE, 18–20 Sept.

Verma, A., and K. Pruess (1988), Thermohydrological conditions and silica redistribution near high-level nuclear wastes emplaced in saturated geological formations, *J. Geophys. Res.*, *93*(B2), 1159–1173, doi:10.1029/JB093iB02p01159.

Zimmerman, R. W., and G. S. Bodvarsson (1996), Hydraulic conductivity of rock fractures, *Transp. Porous Media*, *23*(1), 13–30.

A. Chaudhuri, Department of Applied Mechanics, Indian Institute of Technology Madras, Chennai 36 Tamil Nadu, India.

H. Rajaram, Department of Civil, Environmental and Architectural Engineering, University of Colorado, Boulder, CO 80309, USA.

H. Viswanathan, Earth and Environmental Sciences Division, Los Alamos National Laboratory, Los Alamos, NM 87545, USA.